AIAA JOURNAL
Vol. 42, No. 3, March 2004

Buckling of Laminated Conical Shells Given the Variations of the Stiffness Coefficients

Yiska Goldfeld* and Johann Arbocz†
Delft University of Technology, 2629 HS Delft, The Netherlands

The buckling behavior of filament-wound laminated conical shell is thoroughly investigated by consideration of the variation of the stiffness coefficients. To date, all analyses of laminated conical shells have been undertaken with constant stiffness coefficients in the laminate constitutive relations, usually under the assumption of nominal material properties taken from the midlength of the cone. The main object of the study is to investigate the influence of the variation of the stiffness coefficients on the buckling behavior of laminated conical shells. An analytical and computational model was developed to calculate the variation of the stiffness coefficients under the assumption that, in the case of filament-wound truncated conical shells, the fiber orientation changes using a geodesic path. The model was added to the computer code STAGS-A to calculate the buckling behavior of the laminated conical shell.

Nomenclature

$A_{ij}, \boldsymbol{A}$	=	membrane stiffness coefficients defined by Eq. (21)
$B_{ij}, \boldsymbol{B}$	=	coupling stiffness coefficients defined by Eq. (22)
b_s	=	general distance between fibers defined by Eq. (6)
b_1	=	distance between the longitudinal fibers for $s = s_1$
C	=	$\cos(\beta_k)$ [Eqs. (12)]
$D_{ij}, \boldsymbol{D}$	=	flexural stiffness coefficients defined by Eq. (23)
d_1	=	constant defined by Eq. (4)
E_{11}, E_{22}	=	apparent elastic moduli for an orthotropic lamina
G_{12}	=	apparent shear modulus of an orthotropic lamina
K	=	layer (or lamina) index
L	=	slant length of the conical shell
$\boldsymbol{M}$	=	moment resultants, $\{M_s, M_\theta, M_{s\theta}\}$
N	=	number of layers (or laminae)
$\boldsymbol{N}$	=	force resultants, $\{N_s, N_\theta, N_{s\theta}\}$
N_{xxcr}	=	axial compression buckling load
$N_{x\theta cr}$	=	torsional buckling load
p_{cr}	=	hydrostatic buckling load
$Q_{ij}, \boldsymbol{Q}$	=	coefficients defined by Eqs. (9)
$\bar{Q}_{ij}, \bar{\boldsymbol{Q}}$	=	transformed reduced stiffness, defined by Eqs. (11)
R_1	=	radius at the narrower end of the cone
S	=	$\sin(\beta_k)$ [Eqs. (12)]
s, s_1, s_2	=	longitudinal coordinates for conical surface (Fig. 1)
t_s, t_k	=	thickness of a lamina
t_1	=	thickness of laminated shell at the top of the cone
w	=	radial displacement (positive inward)
x	=	axial coordinate for conical shell (Fig. 1)
z	=	coordinate perpendicular to the shell wall (positive inward)
α	=	cone semivertex angle
β	=	winding angle [Eq. (5)]
β_1	=	winding angle at the top of the cone
$\boldsymbol{\varepsilon}$	=	strains, $\{\varepsilon_s, \varepsilon_\theta, \gamma_{s\theta}\}$
$\boldsymbol{\varepsilon}^0$	=	strains at the reference surface, $\{\varepsilon_s^0, \varepsilon_\theta^0, \gamma_{s\theta}^0\}$
$\varepsilon_1, \varepsilon_2, \gamma_{12}$	=	strains in the direction of the principle axis of a lamina
θ	=	conical circumferential coordinate; coordinate of a fiber [Fig. 1 and Eq. (1)]
ν	=	Poisson's ratio for isotropic sheet
ν_{12}, ν_{21}	=	apparent Poisson's ratios for an orthotropic lamina
$\boldsymbol{\sigma}$	=	stress, $\{\sigma_s, \sigma_\theta, \tau_{s\theta}\}$
$\sigma_1, \sigma_2, \tau_{12}$	=	stress in the direction of the principle axis of a lamina
$\boldsymbol{\chi}$	=	change of curvature and twist of the middle surface, $\{\chi_s, \chi_\theta, \chi_{s\theta}\}$

Introduction

COMPOSITE laminated conical shells are widely used in aeronautic, naval and civil engineering structures. Unlike the isotropic conical shells, in the case of composite laminated materials, the thickness and the material's properties vary with the shell coordinates, which ultimately result in coordinate dependence of the stiffness matrices ($\boldsymbol{A}$, $\boldsymbol{B}$, and $\boldsymbol{D}$). This effect complicates the problem considerably. The first level of complexity is attributed to the need to find an analytic representation of those functions, which depend on many factors such as the manufacturing process, the variation of the angle ply, the change of the shell's thickness, etc. An exhaustive study of the stiffness functions and their dependence on the various factors has been performed by Baruch et al.[1,2] The second level of complexity is associated with the introduction of coordinate dependent stiffness matrices into the mathematical model and the solution of the system of nonlinear governing partial differential equations with variable coefficients. To avoid these obstacles, in most investigations reported in the literature, the stiffness coefficients are assumed constant.

In most of the works that deal with laminated conical shells, there is no consideration of the variation of the stiffness coefficients with the shell coordinates.[3–7] In some cases (Ref. 8, for example), the simplifying assumption of constant stiffnesses throughout the entire shell has been adopted. For example, Tong et al.[9] omitted the influence of the angle variation and adopted the value of the ply angle at the midlength of the cone as the nominal value and considered only linear variation of the thickness of the shell in their proposed solution.

Tong[10] suggested a simple formula for the critical buckling loads of laminated conical shells with stretching–bending coupling under axial compression. His formula is based on Seide's[11] formula for isotropic conical shell and uses constant stiffness. As a result, the model presented by Tong[10] is only suitable for imaginary conical shells that cannot be manufactured in practice (see Baruch[12]).

Baruch et al.[1,2] showed that, due to the unique geometry of the conical surface, and with regards to the filament winding process used in casting of the laminated shell, constant stiffness coefficients

Received 30 May 2003; revision received 22 September 2003; accepted for publication 3 October 2003.

*Postdoctoral Fellow, Faculty of Aerospace Engineering, Kluyverweg 1.
†Professor Emeritus, Faculty of Aerospace Engineering, Kluyverweg 1. Fellow AIAA.

can never be achieved. The stiffnesses of a laminated conical shell always vary and are strongly dependent on the coordinates of the shell. It is also shown that by selection of a proper filament winding process, these functions can be reduced to functions of the longitudinal coordinate only. However, due to the significant complexity involved with analysis of the buckling load and the imperfection sensitivity of such laminated conical shells, Zhang[13] and Zhang and Arbocz[14] omitted the influence of the stiffness variation and used nominal values instead. Khatri and Bardell[15] found that for the case of laminated open conical shell panels built by the use of a different manufacturing process, the stiffness coefficients are also functions of the coordinates. Hence, to quote the conclusion of Baruch et al.[1,2] and Baruch,[16] "The stiffness coefficients needed for the analysis of a laminated structure have to be calculated only after taking into account the process which can be used to build the structure."

An advanced investigation for finding an adequate model for the behavior of the composite shell is reported by Tong.[17,18] Numerical and experimental investigations are presented for laminated conical shells under axial compression and for different ply stacking sequences, whereas a modified model is proposed to calculate the ply thickness. However, here again, the buckling loads have been calculated while both the effect of the ply angle and variation of the ply thickness were neglected and replaced with nominal ones taken from the midlength of the cone.

In this study, laminated conical shells will be thoroughly investigated by consideration of the variation of the stiffness coefficients (A_{ij}, B_{ij}, and D_{ij}) and their dependence on the shell's coordinate. The improvement in this research is achieved by the adoption of a suitable analytical representation to describe the coordinate dependent stiffness and, especially, by the study of the influence of the variation of the stiffness coefficients on the buckling behavior of the filament-wound laminated conical shell. The exact solution was calculated via the computer code STAGS-A[19] by the addition of a user-written subroutine WALL. A comparison between the exact buckling load solution via STAGS-A and the buckling load based on average stiffnesses will be performed to validate the assumption that has been used by many researchers. Furthermore, to try to find a better estimate for the exact buckling load, comparison with the solution derived by the exact stiffnesses at the midlength of the cone will also be carried out. Moreover, in the attempt to find an adequate lower bound to the exact buckling load, the buckling load was also calculated by the use of the stiffness matrices at the large end of the cone (weakest cross section of the shell).

Constitutive Relation of Laminated Conical Shell

Some parts of this section have already been carried out by others; however, for completeness of the subject, they will be repeated here.

Position of the Fiber on Filament-Wound Truncated Circular Conical Shell

The position of a fiber will be defined by setting θ (the conical circumferential coordinate) as a known function of s (the conical longitudinal coordinate) (Fig. 1).

During the filament winding process, a single fiber tow runs repetitively from one pole to the other to form one over-and-under woven fabric layer, which can be approximated as two single plies with fibers equally distributed in both directions, that is, $\pm\beta$. For the case of filament-wound truncated conical shell, the orientation of the fiber is applied by the use of a geodesic path (the shortest distance between two points on a surface). For this case, the fiber's coordinate is given by[1,2]

$$\theta(s) = (1/\sin\alpha)[\arccos(d_1/s) - \arccos(d_1/s_1)] \tag{1}$$

where s_1 is the coordinate at the narrower end of the cone (Fig. 1) and d_1 is a constant that will be defined later.

Because the angle between the fiber and the longitudinal coordinate β is defined as (Baruch et al.[1,2])

$$\tan\beta = s\theta_{,s}\sin\alpha \tag{2}$$

From Eqs. (1) and (2),

$$\sin\beta = (d_1/s) \tag{3}$$

and the initial winding angle at the narrower end of the conical shell ($s = s_1$) is

$$\sin\beta_1 = (d_1/s_1) \tag{4}$$

Therefore, the angle between the fiber and the longitudinal coordinate can be rewritten as

$$\sin\beta = (s_1/s)\sin\beta_1 \tag{5}$$

The distance between the fibers is obtained as (Baruch et al.[1,2])

$$b_s = b_1\frac{s\cos\beta}{s_1\cos\beta_1} \tag{6}$$

where b_1 is the distance between the fibers at the narrower edge of the cone.

Thickness of a Lamina

Because the amount of material for unit length of the fiber is kept constant during the filament winding process, it follows that

$$b_s t_s = b_1 t_1 \rightarrow \text{const} \tag{7}$$

where t_1 is the thickness of the lamina for $s = s_1$.

Equations (6) and (7) yield

$$t_s = t_1\frac{s_1\cos\beta_1}{s\cos\beta} \tag{8}$$

Variation of Fiber Orientations

In Fig. 2 the change of the fiber inclination, the distance between the fibers, and the thickness of the lamina, are plotted vs the longitudinal coordinate for conical shells (with a slant length of $L = 0.2$ m and a shorter radius of the truncated cone $R_1 = 0.1325$ m) with various cone semi-vertex angles (values from $\alpha = 0$ to 90 deg). The angle between the fiber and the longitudinal coordinate at the narrower end of the cone was taken as $\beta_1 = 45$ deg. As was expected, the fiber orientation is highly dependent on the cone semi-vertex angle. The wider the cone semivertex angle, the more the fiber orientation is affected. Furthermore, the most significant discrepancy occurs at small cone semivertex angles. This implies that decreases of the thickness and the ply angle, along with the longitudinal coordinate, is higher between $\alpha = 0$ and 10 deg than, for instance, between $\alpha = 45$ and 90 deg. Moreover, note that the changes of the ply properties, along the longitudinal coordinate, for $\alpha = 45$–90 deg are almost the same, and the wider the cone semivertex angle, the less the discrepancy. The ratios between the thickness at the midlength and at the top of the cone (the narrower end) and between the bottom (the larger end) and the top vs the cone semivertex angle are plotted in Fig. 3. Note that the wider the cone semivertex angles, the higher the discrepancies between the thicknesses. This will mainly influence the discrepancy between the exact buckling loads and the nominal ones, as will be presented later.

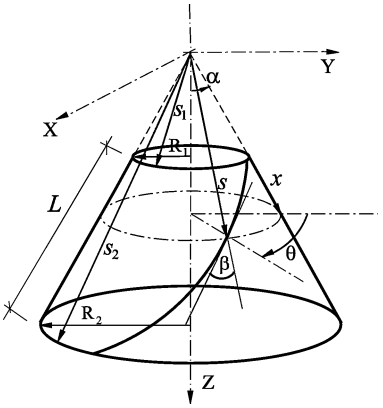

Fig. 1 Geometry and sign convention for coordinates and the position of a fiber on a conical shell.

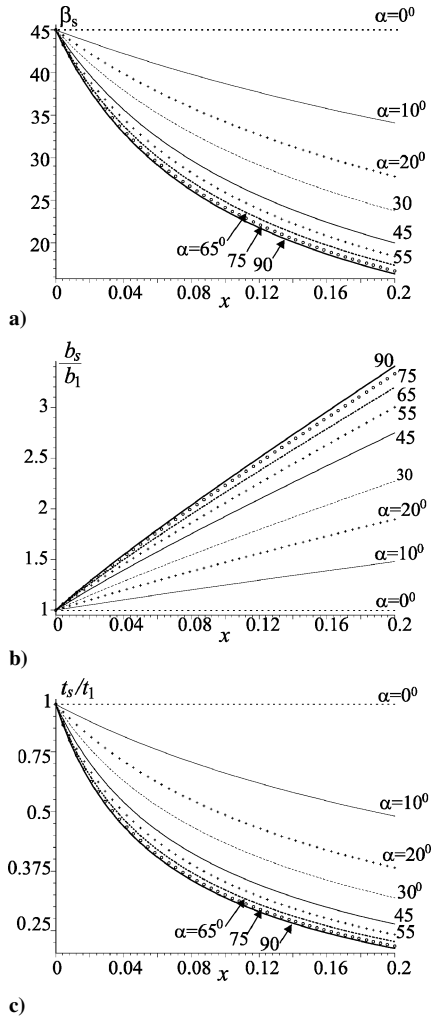

Fig. 2 Change of a) fiber inclination, b) distance between the fibers, and c) thickness of the lamina vs the longitudinal coordinate for filament-wound conical shells with various cone semivertex angles.

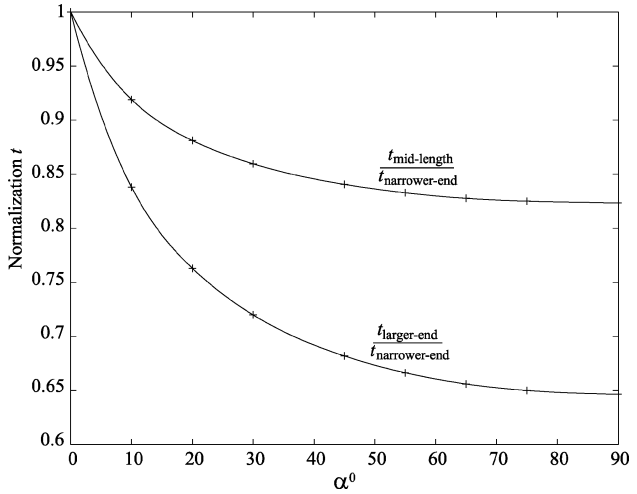

Fig. 3 Change of thickness ratios vs cone semivertex angle.

Stiffness Behavior of a Lamina

Following Jones[20] and Whitney,[21] the constitutive equations for the kth homogeneous orthotropic lamina, with consideration to its principle axis (1, 2), are

$$\begin{Bmatrix}\sigma_1\\ \sigma_2\\ \tau_{12}\end{Bmatrix}_k = \begin{bmatrix}Q_{11} & Q_{12} & 0\\ Q_{12} & Q_{22} & 0\\ 0 & 0 & Q_{66}\end{bmatrix}\begin{Bmatrix}\varepsilon_1\\ \varepsilon_2\\ \gamma_{12}\end{Bmatrix}_k \tag{9}$$

where $Q_{11} = E_{11}/(1-\nu_{12}\nu_{21})$, $Q_{22} = E_{22}/(1-\nu_{12}\nu_{21})$, $Q_{12} = \nu_{21}Q_{11} = \nu_{12}Q_{22}$, and $Q_{66} = G_{12}$. There are four elastic constants: E_{11}, E_{22}, ν_{12}, and G_{12}, whereas ν_{21} is received from the symmetrical demand of the stiffness matrix as $\nu_{12}E_{22} = \nu_{21}E_{11}$.

In the case of laminated conical shells, the lamina principal axes (1, 2) do not coincide with the reference axes of the shell (s, θ). Thus, to be able to determine the shell wall constitutive equations, the constitutive equations for each individual lamina must be transformed to the shell wall reference axes. This transformation yields

$$\begin{Bmatrix}\sigma_s\\ \sigma_\theta\\ \tau_{s\theta}\end{Bmatrix}_k = \begin{bmatrix}\bar{Q}_{11} & \bar{Q}_{12} & \bar{Q}_{16}\\ \bar{Q}_{12} & \bar{Q}_{22} & \bar{Q}_{26}\\ \bar{Q}_{16} & \bar{Q}_{26} & \bar{Q}_{66}\end{bmatrix}\begin{Bmatrix}\varepsilon_s\\ \varepsilon_\theta\\ \gamma_{s\theta}\end{Bmatrix}_k \tag{10}$$

where

$$\begin{aligned}
\bar{Q}_{11} &= Q_{11}C^4 + 2(Q_{12}+2Q_{66})C^2S^2 + Q_{22}S^4\\
\bar{Q}_{12} &= (Q_{11}+Q_{22}-4Q_{66})C^2S^2 + Q_{12}(C^4+S^4)\\
\bar{Q}_{22} &= Q_{11}S^4 + 2(Q_{12}+2Q_{66})C^2S^2 + Q_{22}C^4\\
\bar{Q}_{66} &= (Q_{11}+Q_{22}-2Q_{12}-2Q_{66})C^2S^2 + Q_{66}(C^4+S^4)\\
\bar{Q}_{16} &= (Q_{11}-Q_{12}-2Q_{66})C^3S + (Q_{12}-Q_{22}+2Q_{66})CS^3\\
\bar{Q}_{26} &= (Q_{11}-Q_{12}-2Q_{66})CS^3 + (Q_{12}-Q_{22}+2Q_{66})C^3S
\end{aligned} \tag{11}$$

whereas

$$C = \cos\beta_k, \qquad S = \sin\beta_k \tag{12}$$

In correspondence to the winding process, the $[\bar{\boldsymbol{Q}}]_k$ matrix will change with the changing of the winding angle β_k, which depends on the longitudinal coordinate [Eq. (5)].

The strain–displacement equations are given by

$$\{\varepsilon\} = \{\varepsilon^0\} + z\{\chi\} \tag{13}$$

where $\{\varepsilon\}^T = \{\varepsilon_s, \varepsilon_\theta, \gamma_{s\theta}\}$, $\{\varepsilon^0\}^T = \{\varepsilon_s^0, \varepsilon_\theta^0, \gamma_{s\theta}^0\}$ and $\{\chi\}^T = \{\chi_s, \chi_\theta, \chi_{s\theta}\}$.

Substituting Eq. (13) into Eq. (10) yields

$$\{\sigma\}_k = [\bar{\boldsymbol{Q}}]_k\{\varepsilon^0\} + z[\bar{\boldsymbol{Q}}]_k\{\chi\} \tag{14}$$

Stress and Moment Resultants of the Laminate

For thin-walled shells, the stress and moment resultants acting at the shell mid-surface are obtained by integration of the stresses in each layer (or lamina) through the laminate thickness as

$$\{\boldsymbol{N}\} = \sum_{k=1}^{N}\int_{t_{k-1}}^{t_k}\{\sigma\}_k\,\mathrm{d}z \tag{15}$$

$$\{\boldsymbol{M}\} = \sum_{k=1}^{N}\int_{t_{k-1}}^{t_k}\{\sigma\}_k z\,\mathrm{d}z \tag{16}$$

where $\{\boldsymbol{N}\}^T = \{N_s, N_\theta, N_{s\theta}\}$ and $\{\boldsymbol{M}\}^T = \{M_s, M_\theta, M_{s\theta}\}$, whereas the position of the kth lamina is defined by $t_{k-1} < z < t_k$ and N is the number of laminaes.

Note that $\{\varepsilon^0\}$ and $\{\chi\}$ are not functions of z, and, within any layer (from t_{k-1} to t_k), $[\bar{\boldsymbol{Q}}]_k$ is also not a function of z. Then, substitution of Eq. (14) into Eqs. (15) and (16) yields

$$\{\boldsymbol{N}\} = \sum_{k=1}^{N}\left([\bar{\boldsymbol{Q}}]_k\{\varepsilon^0\}\int_{t_{k-1}}^{t_k}\mathrm{d}z + [\bar{\boldsymbol{Q}}]_k\{\chi\}\int_{t_{k-1}}^{t_{k+1}} z\,\mathrm{d}z\right) \tag{17}$$

$$\{\boldsymbol{M}\} = \sum_{k=1}^{N}\left([\bar{\boldsymbol{Q}}]_k\{\varepsilon^0\}\int_{t_{k-1}}^{t_k} z\,\mathrm{d}z + [\bar{\boldsymbol{Q}}]_k\{\chi\}\int_{t_{k-1}}^{t_{k+1}} z^2\,\mathrm{d}z\right) \tag{18}$$

Furthermore, $\{\varepsilon^0\}$ and $\{\chi\}$ are not functions of k, and, thus, Eqs. (17) and (18) can be reduced to the following form:

$$\{N\} = [A]\{\varepsilon^0\} + [B]\{\chi\} \tag{19}$$

$$\{M\} = [B]\{\varepsilon^0\} + [D]\{\chi\} \tag{20}$$

where

$$A = \sum_{k=1}^{N} [\bar{Q}]_k (t_k - t_{k-1}) \tag{21}$$

$$B = \frac{1}{2} \sum_{k=1}^{N} [\bar{Q}]_k \left(t_k^2 - t_{k-1}^2\right) \tag{22}$$

$$D = \frac{1}{3} \sum_{k=1}^{N} [\bar{Q}]_k \left(t_k^3 - t_{k-1}^3\right) \tag{23}$$

As has been shown earlier, the winding angle β_k of a conical shell depends on the winding process, and it is a function of the longitudinal coordinate (s). Furthermore, the thickness of the lamina also changes in the longitudinal direction. Therefore, the [A], [B], and [D] matrices are strong functions of s.

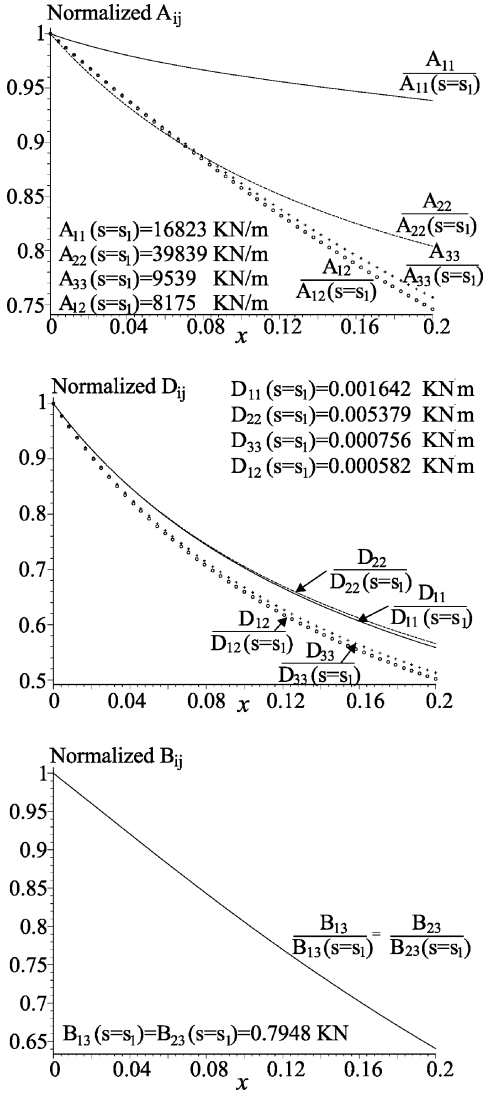

Fig. 4 Change of stiffness coefficients for GFRP filament-wound conical shell ($\alpha = 9$ deg, $L = 0.2$ m, and $R_1 = 0.1325$ m).

Variation of the Stiffness Coefficients

In Fig. 4 the coefficients A_{ij}, B_{ij}, and D_{ij} are plotted vs the longitudinal coordinate for Tong's[17,18] glass fiber reinforced plastic (GFRP) conical shell ($\alpha = 9$ deg, $R_1 = 0.1325$ m, and $L = 0.2$ m) with material properties as follows: The longitudinal modulus $E_{11} = 42.6$ GPa; the transverse modulus $E_{22} = 11.7$ GPa; the shear modulus $G_{12} = 4.8$ GPa; and Poisson's ratio $\nu_{12} = 0.302$. The fiber orientation at the midlength of the cone is (90/±45/90 deg), and the thickness at the narrower end $t_1 = 1.16$ mm. Note that all stiffness coefficients are affected by the fiber orientation. The stiffness coefficients decrease by approximately ~60% from the top of the cone (narrower end) to the bottom (larger end). The variation is most pronounced for D_{ij}, a reduction of 50%, because for this case the thickness is raised to the power of three in Eq. (23). Furthermore, as the cone semivertex angle increases, the reduction of the stiffness coefficients also increases, as can be seen in Fig. 5, for the GFRP conical shell [with layups of (90/±45/90 deg) at the narrower end of the shell]. Here again, the most significant discrepancy occurs at small cone semivertex angle. This means that the decreases of the stiffness coefficients, with the longitudinal coordinate, is higher between $\alpha = 0$ and 10 deg than between $\alpha = 45$ and 90 deg. In all cases, the most compliant part of the shell is in the larger end of the cone where the inclination of the fibers, and especially the thickness, are the smallest.

Buckling Load of Filament-Wound Laminated Conical Shells

The main objective of this study is the investigation of the influence of the variation of the stiffness coefficients on the buckling behavior of filament-wound truncated conical shells. In addition, the appropriate range for the validity of the various approximate solutions is established by comparison with the exact buckling load. The exact buckling load is calculated taking into account the variations of the stiffness matrices. The approximate solutions are obtained under the assumption of constant stiffness matrices based on material properties taken from different shell cross sections, as follows:

1) Buckling load based on average stiffnesses is the most common calculation in the literature. It uses an average thickness (from both ends of the shell), under the assumption that each ply had an equal thickness and takes the fiber inclination from the midlength of the shell.

2) Buckling load based on exact stiffnesses at the midlength is calculated by the use of the exact thickness of each ply at the midlength of the shell and by the use of the fiber inclination from the midlength of the shell.

3) Buckling load based on stiffnesses at the large end is calculated by the use of the thickness from the larger end of the cone, under the assumption that each ply had an equal thickness, and by the use of the fiber inclination, also from the large end of the cone.

The exact buckling load was computed by the inclusion of the variation of the stiffness coefficients. This was done with the computer code STAGS-A,[19] by addition of a user-written subroutine, WALL. Subroutine WALL makes it possible to vary the stiffness matrices or the material properties that influence the calculation of the stiffness matrices at each mesh point. In this work, subroutine WALL was written for the case of filament-wound truncated circular conical shells under the assumption that the fiber orientation changes as a geodesic path.

To validate the result and to check the accuracy of the buckling loads, they were calculated by a linear bifurcation analysis and by nonlinear bifurcation analysis.

Results and Discussion

Initially, filament-wound truncated circular conical shells made of GFRP were examined. The geometric and material properties were taken from Refs. 17 and 18, as mentioned before. The cone semivertex angle changes from $\alpha = 0$ deg (cylindrical shell) to $\alpha = 90$ deg (annular plate). The fiber orientation at the narrower end of the cone was taken as (90/±45/90 deg), and the thickness $t_1 = 1.16$ mm. The fiber orientations and the thicknesses at the various cross sections are

Table 1 Wall thicknesses and fiber orientation at various cross sections of filament-wound conical shells

	Average material properties		Exact material properties at the midlength		Material properties at the large end	
α	t_{average}, mm	(90 deg/$\pm\beta$ deg$_{\text{midlength}}$/90 deg)	$0.29/t_k/t_k/0.29$, mm	(90 deg/$\pm\beta$ deg$_{\text{midlength}}$/90 deg)	t_{bottom}, mm	(90 deg/$\pm\beta$ deg$_{\text{bottom}}$/90 deg)
0	1.160	45	0.29	45	1.16	45
10	1.066	38.69	0.2323	38.69	0.972	34.07
20	1.022	34.19	0.1970	34.19	0.885	27.79
30	0.997	30.88	0.1734	30.88	0.835	23.76
45	0.975	27.45	0.1506	27.45	0.791	20.00
55	0.966	25.91	0.1408	25.91	0.773	18.43
65	0.960	24.82	0.1342	24.82	0.761	17.37
75	0.957	24.14	0.1299	24.14	0.754	16.71
85	0.955	23.80	0.1279	23.80	0.751	16.41
90	0.955	23.76	0.1276	23.76	0.750	16.40

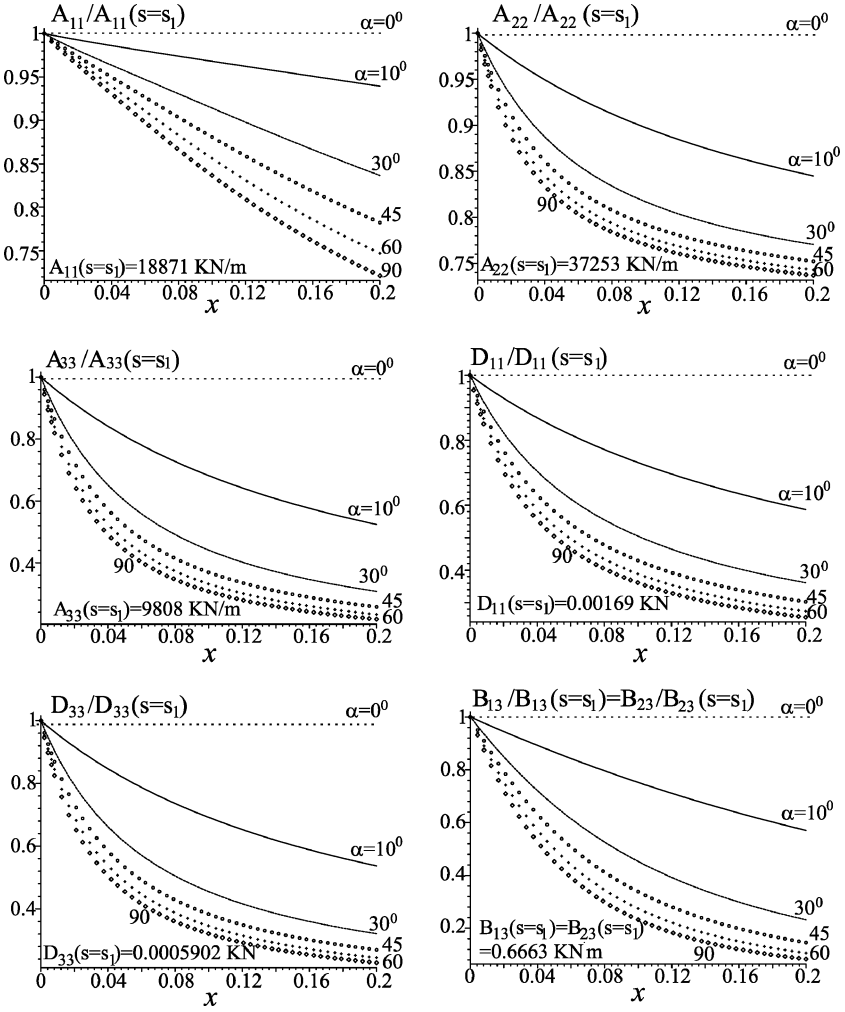

Fig. 5 Change of stiffness coefficients for GFRP filament-wound conical shells with different cone semi-vertex angles.

listed in Table 1. The study covered axial compression, hydrostatic pressure, and torsion.

Axial Compression

The axial compression was applied through the boundary conditions, at the narrower end SS3, that is, $N_{xx} = \bar{N}_{xx}$ and $v = w = M_{xx} = 0$, and at the larger end SS4, that is, $w = M_{xx} = v = u = 0$, where N_{xx} is the axial stress resultant. The results are listed in Table 2. Note that in all cases, the exact buckling loads are less than the ones based on average stiffness. The discrepancy between them is mostly affected by the changes of the thickness, which is influenced by the cone semivertex angle, as can be seen in Fig. 3. The wider the cone semivertex angles, the higher the relative discrepancy between the exact buckling load and the buckling load based on average stiffnesses.

Furthermore, in all cases, the exact buckling loads were higher than the buckling loads based on stiffnesses at the large end of the cone (Fig. 6). One could say that for a filament-wound conical shell under axial compression, buckling load based on stiffnesses at the large end of the cone is a lower bound for the exact buckling load. To be on the safe side, calculation of the buckling load by the assumption of constant stiffness matrices should be carried out with the material properties taken from the large end of the cone (the weakest cross section). However, the discrepancy between the buckling load based on stiffness at the large end and the exact buckling load could be up to ~35%, whereas the discrepancy between the exact buckling load and the one based on average stiffnesses is only up

Table 2 Buckling load based on exact stiffnesses, average stiffnesses, exact stiffnesses at the midlength, and stiffnesses at the large end of laminated conical shells under axial compression[a]

	Exact buckling load, kN/m		Buckling load based on average stiffnesses, kN/m		Buckling load based on exact stiffnesses at the midlength, kN/m		Buckling load based on stiffnesses at the large end, kN/m	
α	Linear bifurcation	Nonlinear bifurcation analysis	Linear bifurcation	Nonlinear bifurcation analysis	Linear bifurcation	Nonlinear bifurcation analysis	Linear bifurcation	Nonlinear bifurcation analysis
0	106.89 (9, 9)	103.08 (9, 9)	106.89(9, 9)	103.08 (9, 9)	106.89 (9, 9)	103.08 (9, 9)	106.89 (9, 9)	103.08 (9, 9)
10	74.54 (5, 11)	74.41 (6, 11)	86.0 (9, 10)	86.04 (8, 10)	82.590 (9, 10)	82.276 (9, 10)	69.94 (9, 11)	69.58 (8, 11)
20	59.18 (6, 12)	57.99 (4, 13)	73.84 (8, 10)	68.94 (8, 10)	67.228 (8, 11)	64.185 (6, 10)	53.92 (7, 12)	48.48 (3, 11)
30	48.13 (5, 13)	47.12 (5, 13)	63.93 (8, 10)	54.90 (4, 10)	55.551 (8, 12)	49.903 (4, 10)	43.72 (7, 13)	36.18 (4, 10)
45	35.38 (4, 13)	34.71 (4, 13)	49.62 (6, 10)	42.68 (4, 9)	41.067 (6, 12)	33.712 (2, 10)	32.12 (6, 12)	25.49 (2, 10)
55	27.83 (4, 12)	27.38 (4, 12)	39.69 (5, 9)	33.87 (4, 8)	32.138 (5, 11)	26.773 (4, 9)	25.19 (6, 12)	18.62 (4, 8)
65	20.42 (3, 10)	20.08 (3, 11)	29.21 (5, 8)	25.09 (4, 7)	23.328 (5, 9)	17.633 (3, 10)	18.36 (4, 10)	15.10 (2, 8)
75	12.66 (3, 8)	12.69 (3, 9)	18.13 (4, 6)	15.33 (3, 6)	14.388 (4, 7)	10.346 (3, 6)	11.35 (4, 7)	9.248 (3, 4)
90	0.508 (1, 0)	0.508 (1, 0)	0.647 (1, 0)	0.647 (1, 0)	0.4329 (1, 0)	0.4329 (1, 0)	0.320 (1, 0)	0.320 (1, 0)

[a]Numbers in parentheses: (axial half-wave number, circumferential wave number).

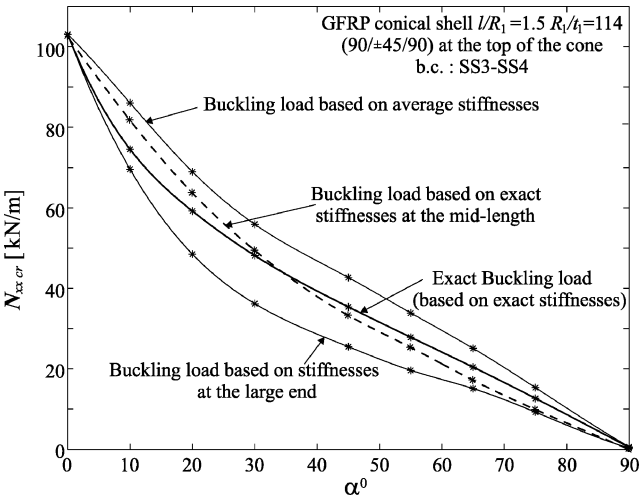

Fig. 6 Buckling loads vs cone semivertex angle for different stiffness matrices for conical shell under axial compression.

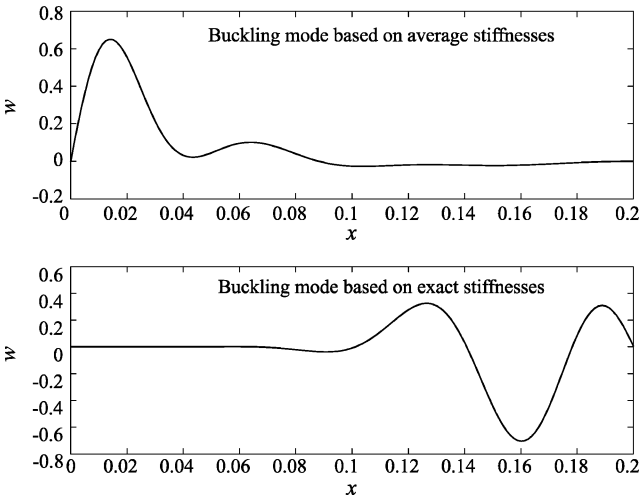

Fig. 7 Buckling modes of filament-wound conical shell, $\alpha = 45$ deg, with different stiffness matrices and under axial compression.

to ~20% (annular plate in both cases). This implies that the buckling load based on the average stiffnesses gives a better estimate for the exact buckling load, but, nevertheless, it is not on the safe side. The buckling load based on the exact stiffness at the midlength was also computed (Table 2 and the dashed line in Fig. 6). Note that the buckling load based on the exact stiffnesses at the midlength gives a better estimate for the exact buckling load. However, for small cone semivertex angles ($\alpha <\sim 40$ deg), the exact stiffnesses give a value above the exact buckling load (nonconservative) and for wider cone semivertex angles, that value is below (conservative).

It is seen that there is a good agreement between the buckling loads computed by the linear and nonlinear bifurcation analyses. However, the buckling modes, in some cases, are slightly different. This is probably a result of satisfaction of the nonlinear edge constraints in the nonlinear bifurcation analysis.

Not only is the buckling load different, but the buckling mode is too. Usually, exact solution of the buckling behavior with the variable stiffness coefficients yields higher circumferential wave numbers than solutions based on average stiffness or exact stiffness at the midlength, and lower values than the one based on the stiffness at the large end. Wave numbers can be seen in parentheses in Table 2. Furthermore, at the axial direction, the buckling mode of conical shell with constant stiffness matrices usually is concentrated at the narrower end of the shell, dependent on the cone semivertex angle, whereas consideration of the variable stiffness matrices yields a deformation of the buckling mode concentrated at the larger end of the shell, where the thickness is the smallest, as can be seen in Fig. 7 for a conical shell with $\alpha = 45$ deg.

The differences in the buckling mode could affect the postbuckling behavior of the shell and, as a result, affect the imperfection sensitivity of the shell. This must be taken into consideration when laminated conical shells are designed under the assumption that the stiffness coefficients are constant.

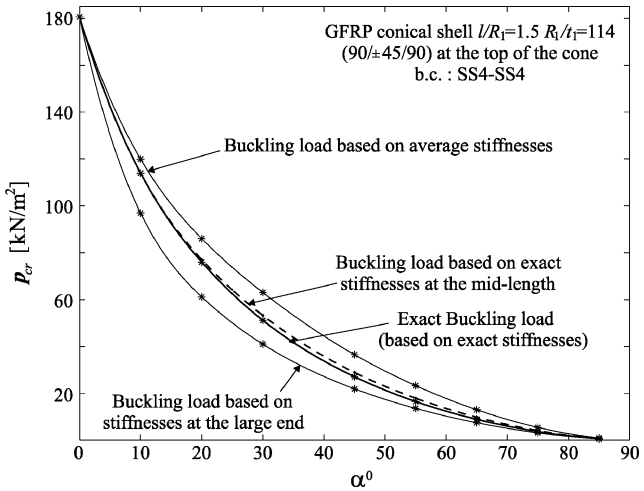

Fig. 8 Hydrostatic buckling loads vs cone semivertex angle for different stiffness matrices.

Hydrostatic Pressure

The hydrostatic pressure was applied to a conical shell with simply supported boundary conditions (SS4 at both ends, that is, $u = v = w = M_{xx} = 0$). In Table 3 and in Figure 8, the buckling loads

Table 3 Buckling load based on exact stiffnesses, average stiffnesses, exact stiffnesses at the midlength and stiffnesses at the large end of laminated conical shells under hydrostatic pressure[a]

	Exact buckling load, kN/m^2		Buckling load based on average stiffnesses, kN/m^2		Buckling load based on exact stiffnesses at the midlength, kN/m^2		Buckling load based on stiffnesses at the large end, kN/m^2	
α	Linear bifurcation	Nonlinear bifurcation analysis	Linear bifurcation	Nonlinear bifurcation analysis	Linear bifurcation	Nonlinear bifurcation analysis	Linear bifurcation	Nonlinear bifurcation analysis
0	179.83 (7)	180.61 (7)	179.83 (7)	180.61 (7)	179.83 (7)	180.61 (7)	179.83 (7)	180.61 (7)
10	113.82 (8)	113.91 (8)	118.94 (8)	119.91 (8)	113.89 (8)	113.98 (8)	96.805 (8)	96.893 (8)
20	75.962 (9)	75.974 (9)	85.960 (9)	85.972 (9)	77.044 (9)	77.054 (9)	61.120 (9)	61.129 (9)
30	51.136 (10)	51.153 (10)	63.014 (9)	63.035 (9)	53.232 (9)	53.249 (9)	40.970 (10)	40.983 (10)
45	27.047 (11)	27.080 (11)	36.464 (10)	36.489 (10)	28.874 (10)	28.893 (10)	21.908 (10)	21.925 (10)
55	16.466 (11)	16.490 (11)	23.275 (10)	23.303 (10)	17.906 (10)	17.929 (10)	13.554 (10)	13.574 (10)
65	8.8947 (10)	8.9207 (10)	12.973 (9)	13.004 (9)	9.8191 (9)	9.8488 (9)	7.447 (10)	7.469 (10)
75	3.6881 (9)	3.6875 (9)	5.4556 (8)	5.4705 (8)	4.0770 (8)	4.0997 (8)	3.1026 (8)	3.1289 (8)
85	0.6335 (6)	0.6277 (6)	0.9350 (5)	0.9313 (5)	0.6894 (6)	0.6856 (6)	0.5050 (6)	0.5030 (6)

[a]Numbers in parentheses: (circumferential wave number), axial wave number = 1.

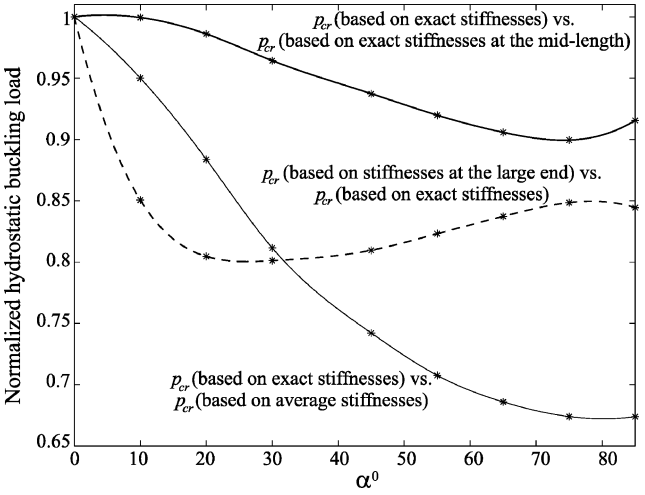

Fig. 9 Normalized hydrostatic buckling loads vs cone semivertex angle.

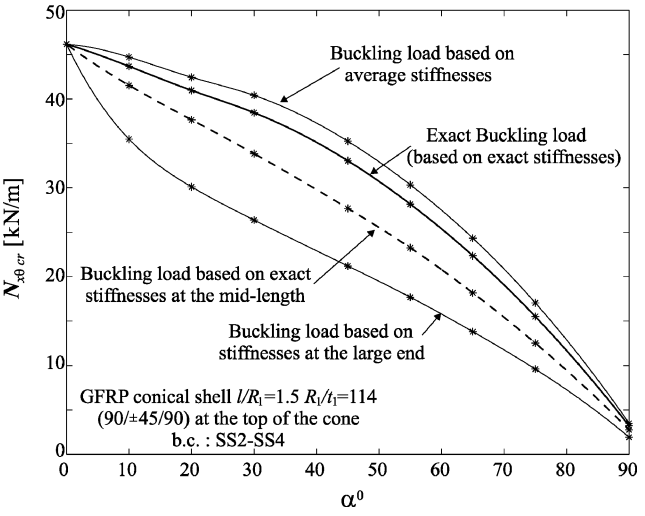

Fig. 10 Torsional buckling loads vs cone semivertex angle for different stiffness matrices.

and the buckling modes are listed (Table 3) and plotted (Fig. 8) for the various solutions. (The circumferential wave numbers are in parentheses, and the axial wave numbers for all cases are a half-wave.) Here again, the exact buckling loads lie between the buckling load based on average stiffness as an upper limit and the buckling load based on stiffness at the large end as a lower limit. The buckling loads based on the exact stiffnesses at the midlength, the dashed line in Fig. 8, are somewhat above the exact loads and give a better estimate of them. Figure 9 shows the ratios between the different buckling loads. One could say that, for the case of laminated conical shell under hydrostatic pressure, solution of the buckling load by the use of the exact stiffness at the midlength could be an appropriate evaluation for the exact buckling load, but that the solution is not on the safe side. It is also seen from Fig. 9 that as the cone semivertex angle becomes larger, the discrepancy between the different buckling loads increases.

Furthermore, the buckling modes, calculated by the use of the different stiffness matrices, vary considerably. The axial buckling modes are the same and consist of a half-wave. The discrepancy is most pronounced in the circumferential direction, and, as the cone semi-vertex angle becomes wider, the discrepancy between the circumferential wave numbers increases. This discrepancy could lead to a different postbuckling behavior and must be taken into consideration when buckling loads are calculated by the use of constant stiffness matrices.

Torsion

The torsional load was applied through the boundary conditions, at the narrower end SS2, that is, $N_{x\theta} = \bar{N}_{x\theta}$ and $u = w = M_{xx} = 0$, and at the larger end SS4, that is, $w = M_{xx} = v = u = 0$, where $N_{x\theta}$ is the shear stress resultant. In Table 4 the torsional buckling loads and modes (in parentheses) are listed. The results are also plotted in Figs. 10 and 11. Here again, the buckling loads based on the stiffnesses at the large end form a lower bound to the exact buckling loads, whereas the buckling loads based on the average stiffnesses form an upper bound. The buckling loads based on exact stiffness at the midlength of the cone, the dashed line in Fig. 10, lie below the exact buckling load for all cone semivertex angles, and the line

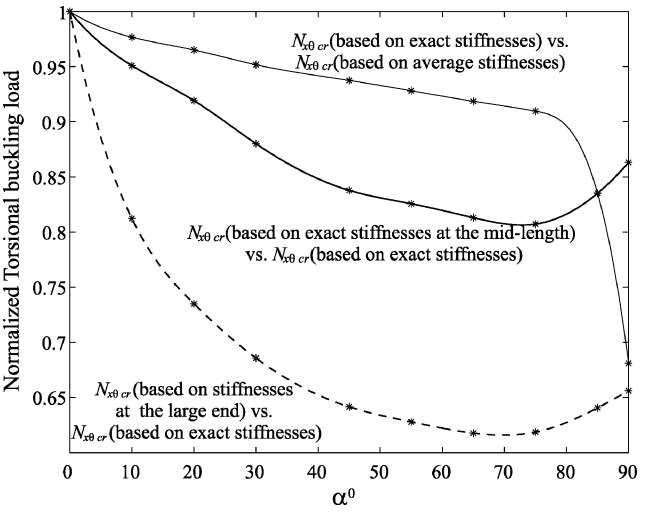

Fig. 11 Normalized torsional buckling loads vs cone semivertex angle.

Table 4 Buckling load based on exact stiffnesses, average stiffnesses, exact stiffnesses at the midlength, and stiffnesses at the large end of laminated conical shells under torsion[a]

	Exact buckling load, kN/m		Buckling load based on average stiffnesses, kN/m		Buckling load based on the exact stiffnesses at the midlength, kN/m		Buckling load based on stiffnesses at the large end, kN/m	
α	Linear bifurcation	Nonlinear bifurcation analysis	Linear bifurcation	Nonlinear bifurcation analysis	Linear bifurcation	Nonlinear bifurcation analysis	Linear bifurcation	Nonlinear bifurcation analysis
0	46.18 (3, 8)	46.17 (3, 8)	46.18 (3, 8)	46.17 (3, 8)	46.18 (3, 8)	46.17 (3, 8)	46.18 (3, 8)	46.17 (3, 8)
10	——	43.68 (3, 9)	45.88 (3, 9)	44.72 (3, 9)	41.53 (3, 9)	41.54 (3, 9)	35.47 (3, 10)	35.48 (3, 10)
20	——	40.97 (3, 10)	42.44 (3, 10)	42.45 (3, 10)	37.65 (3, 10)	37.66 (3, 10)	30.07 (3, 10)	30.11 (3, 10)
30	37.80 (3, 10)	38.46 (3, 10)	40.39 (3, 10)	40.41 (3, 10)	33.84 (3, 10)	33.85 (3, 10)	26.34 (3, 10)	26.37 (3, 10)
45	32.37 (3, 10)	33.05 (3, 10)	35.25 (3, 10)	35.25 (3, 10)	27.68 (3, 10)	27.69 (3, 10)	21.19 (2, 10)	21.20 (3, 10)
55	27.51 (3, 10)	28.16 (3, 10)	30.32 (3, 9)	30.34 (3, 9)	22.65 (2, 10)	23.25 (2, 10)	17.68 (2, 10)	17.68 (2, 10)
65	21.71 (3, 9)	22.36 (3, 9)	24.32 (3, 8)	24.34 (3, 8)	18.18 (3, 9)	18.18 (3, 9)	13.81 (3, 9)	13.81 (3, 9)
75	14.99 (2, 8)	15.51 (2, 8)	17.04 (3, 7)	17.05 (3, 7)	12.52 (2, 7)	12.52 (2, 7)	9.595 (2, 7)	9.594 (2, 7)
85	7.016 (2, 5)	7.241 (2, 5)	8.661 (2, 5)	8.668 (2, 5)	6.046 (2, 5)	6.047 (2, 5)	4.634 (2, 5)	4.638 (2, 5)
90	——	3.201 (1, 2)	——	4.703 (2, 3)	——	2.763 (1, 2)	——	1.928 (1, 2)

[a]Numbers in parentheses: (axial half-wave number, circumferential wave number).

defines an improved lower bound. Furthermore, the buckling load based on average stiffness gives an adequate estimate of the exact one. The maximum discrepancy is approximately 5% (except for large cone semivertex angles, near the annular plate), and the value is on the safe side.

However, as in the preceding load cases, the buckling modes, computed by the use of the different stiffness matrices, are quite different, especially in the circumferential direction and for wider cone semivertex angles. This could lead to a different postbuckling behavior that influences the imperfection sensitivity.

Conclusions

In this study, the filament-wound laminated conical shell is thoroughly investigated under the assumption that fiber orientation changes as a geodesic path. First the influence of the geometrical and elastic parameters on the coordinate-dependent constitutive relations was examined, and then the buckling behavior was investigated by the use of those relations.

From the results presented, the following conclusions can be drawn:

1) The material properties, fiber inclinations, and the thickness of laminated conical shells are strong functions of the longitudinal coordinate that ultimately influences the stiffness coefficients. The dependence on the coordinates also occurs for shells with small cone semivertex angles, consequently, in all cases it must not be neglected and must be taken into consideration.

2) In all cases, buckling loads based on exact solution are bounded by buckling loads based on stiffnesses at the large end from below and by buckling loads based on average stiffnesses from above. This implies that the buckling load based on stiffnesses at the large end correspond to the lower limit of the exact buckling load and that the buckling load based on average stiffnesses correspond to the upper limit. However, the buckling modes are quite different, which may imply different postbuckling behavior.

3) The buckling loads based on exact stiffness at the midlength sometimes give a better estimate for the exact buckling loads. However, in some cases, it is higher than the exact buckling load (nonconservative), and this must be taken into consideration.

4) The exact buckling behavior is different from the nominal ones. Not only the buckling loads but also the buckling modes are different. This could influence the postbuckling behavior and, as a result, influence the imperfection sensitivity of the shell. Hence, the differences in the buckling modes must be taken into consideration.

References

[1]Baruch, M., Arbocz, J., and Zhang, G. Q., "Laminated Conical Shells—Considerations for the Variations of Stiffness Coefficients," Faculty of Aerospace Engineering, Rept. LR-671, Delft Univ. of Technology, Delft, The Netherlands, April 1992.

[2]Baruch, M., Arbocz, J., and Zhang, G. Q., "Laminated Conical Shells—Considerations for the Variations of the Stiffness Coefficients," *Proceedings of the 35th AIAA/ASME/ASCE/AHS/ASC Structures, Structural Dynamics, and Materials Conference*, AIAA, Washington, DC, 1994, pp. 2505–2516.

[3]Wang, H., and Wang, T. K., "Stability of Laminated Composite Circular Conical Shells Under External Pressure," *Applied Mathematics and Mechanics*, Vol. 12, No. 12, 1991, pp. 1153–1161 (English ed.).

[4]Tong, L., and Wang, T. K., "Simple Solutions for Buckling of Laminated Conical Shells," *International Journal of Mechanics Science*, Vol. 34, No. 2, 1992, pp. 93–111.

[5]Tong, L., and Wang, T. K., "Buckling Analysis of Laminated Composite Conical Shells," *Composites Science and Technology*, Vol. 1, No. 47, 1993, pp. 57–63.

[6]Li, L., "The Stability of Composite Material Stiffened Conical Shells Under Axial Compression," *Composite Structures*, Vol. 38, No. 1–4, 1997, pp. 169–177.

[7]Tan, T., "Torsional Buckling Analysis of Thin and Thick Shells of Revolution," *International Journal of Solids and Structures*, Vol. 37, 2000, pp. 3055–3078.

[8]Di Sciuva, M., and Icardi, U., "On the Buckling Analysis of Imperfect Laminated Stiffened Conical Shells," *XII Congresso Nazionale A.I.D.A.A.*, 1993.

[9]Tong, L., Tabarrok, B., Xiong, Y., and Wang, T. K., "Buckling Analysis of Axially Compressed Composite Conical Shells with Varying Stiffness," *Proceeding of the First Canadian International Composite Conference and Exhibition*, Montreal, Sept. 1991, pp. 536–544.

[10]Tong, L., "Buckling Load of Composite Conical Shells Under Axial Compression," *Journal of Applied Mechanics*, Vol. 61, 1994, pp. 718–719.

[11]Seide, P., "Axisymmetrical Buckling of Circular Cones Under Axial Compression," *Journal of Applied Mechanics*, Vol. 23, 1956, pp. 625–628.

[12]Baruch, M., "Buckling of Composite Conical Shells," *Journal of Applied Mechanics*, Vol. 62, 1995, p. 551.

[13]Zhang, G. Q., "Stability Analysis of Anisotropic Conical Shells," Ph.D. Dissertation, Faculty of Aerospace Engineering, Delft Univ. of Technology, Delft Univ. Press, Delft, The Netherlands, 1993.

[14]Zhang, G. Q., and Arbocz, J., "Initial Postbuckling Analysis of Anisotropic Conical Shells," *Proceedings of the 34th AIAA/ASME/ASCE/AHS/ASC Structures, Structural Dynamics, and Materials Conference*, AIAA, Washington, DC, 1993, pp. 326–335.

[15]Khatri, K. N., and Bardell, N. S., "The Variation of the Stiffness Coefficients for Laminated Open Conical Shell Panels," *Composite Structures*, Vol. 32, 1995, pp. 287–292.

[16]Baruch, M., "Letter to the Editor: Comment on 'The Variation of the Stiffness Coefficients for Laminated Open Conical Shell Panels,'" *Composite Structures*, Vol. 34, 1996, p. 357.

[17]Tong, L., "Buckling of Filament Wound Composite Conical Shells Under Axial Compression," *Proceedings of the AIAA/ASME/ASCE/AHS/ASC Structures, Structural Dynamics, and Materials Conference Proceeding and Exhibit*, Pt. 1, AIAA, Reston, VA, 1998, pp. 585–594.

[18]Tong, L., "Buckling of Filament-Wound Laminated Conical Shells Under Axial Compression," *AIAA Journal*, Vol. 37, No. 6, 1999, pp. 778–781.

[19]Almroth, B. O., Brogan, F. A., Meller, E., Zele, F., and Petersen, H. T., "Collapse Analysis for Shells of General Shape," *User's Manual for the STAGS-A Computer Code*, U.S. Air Force Flight Dynamics Lab., TR AFFDL TR-71-8, Wright–Patterson AFB, OH, 1973.

[20]Jones, R. M., *Mechanics of Composite Materials*, McGraw–Hill, New York, 1975, Chap. 4.

[21]Whitney, J. M., *Structural Analysis of Laminated Anisotropic Plates*, Technomic, Lancaster, PA, 1987.

A. Berman
Associate Editor